

Prediction of Electromagnetic Interference between Antennas on Vehicles

Jiawei Zang*, Xuetian Wang, and Hongmin Gao

Abstract—A simple but efficient method is investigated for predicting electromagnetic interference between antennas on vehicles. By modeling the vehicle body with a conducting wedge, the geometrical optics and uniform theory of diffraction are used to predict the interference power. Comparisons show that the interference power can be accurately predicted with only four dominating rays taken into account. The presented method is validated by measurements in typical environments. A further investigation of various parameters considered in predictions is also presented. Based on the proposed method, the interference power can be easily predicted just in MATLAB instead of the time-consuming full-wave simulation of the entire large-scale structure.

1. INTRODUCTION

In modern transportation, with the application of intelligent traffic management and traffic safety enhancement, more and more antennas are used on vehicles. The transmitted power from these antennas is likely to interfere with other vehicles nearby, causing the problem of electromagnetic interference (EMI). With the rapid development of intelligent vehicle and self-driving, the issue of EMI from antennas on vehicles should be taken seriously.

The authors of [1] investigate the RF exposure inside and outside a cabin in details by considering the vehicle body as a cavity. The approach of eigenmode analysis is adopted, and it requires less computational resources. In [2, 3], the reciprocity theory is used to predict the interference, which significantly reduces the computation time. In [4–8], the researchers focus on estimating interference on a complex platform. The issue of EMI from vehicles in oncoming lanes is discussed in [9]. The two-ray theory (direct and ground-reflected rays) is used to calculate the interference. That means only the effect of the ground on wave propagation is considered; the effect of the platforms (vehicles) on wave propagation is ignored. In [10], the problem of EMI in several typical road traffic scenarios is investigated. In addition to the direct ray, the reflected rays induced by ground and cars on the road are also considered. Similarly, the effect of the transmitting and victim platforms on wave propagation is not included.

In this paper, we investigate the issue of EMI between antennas on vehicles based on the geometrical optics (GO) and uniform theory of diffraction (UTD), which includes the effect of platforms and ground environment. The platform is modeled by a conducting wedge, and the ground environment is modeled by its corresponding constitutive parameters: relative permittivity ϵ_r and conductivity σ . We compare the results using seven rays with the results only using the dominating four rays and find that the use of four rays is adequate enough to predict EMI. The presented four-ray model is validated by measurements in two typical environments. After validating the presented method, the influence of vehicle height, antenna height, ϵ_r , and σ on the received interference power is also studied.

Received 22 June 2017, Accepted 6 September 2017, Scheduled 8 September 2017

* Corresponding author: Jiawei Zang (jiaweizang@gmail.com).

The authors are with the School of Information and Electronics, Beijing Institute of Technology, Beijing 100081, China.

2. METHOD AND VALIDATION

For simplicity and without loss of generality, a dipole mounted on the middle of a van is assumed to be the transmitting vehicle, and the victim vehicle has the same configuration. Figure 1 presents geometry view of ray paths. The width and height of the van are W_v and H_v , respectively; H_a denotes antenna height above the roof; d is the distance between the vans. The van body is modeled by a conducting wedge with the interior angle to be 90° . It can be seen that the following four rays: direct ray TR , ground-reflected ray TOR , roof-diffracted ray TQ_1R , and roof-diffracted ray TQ_2R are considered in Figure 1(a). Additional three second-order rays are shown in Figure 1(b), which includes roof-diffracted-ground-reflected ray TQ_1O_1R , ground-reflected-roof-diffracted ray TO_2Q_2R , and double diffraction ray TQ_1Q_2R .

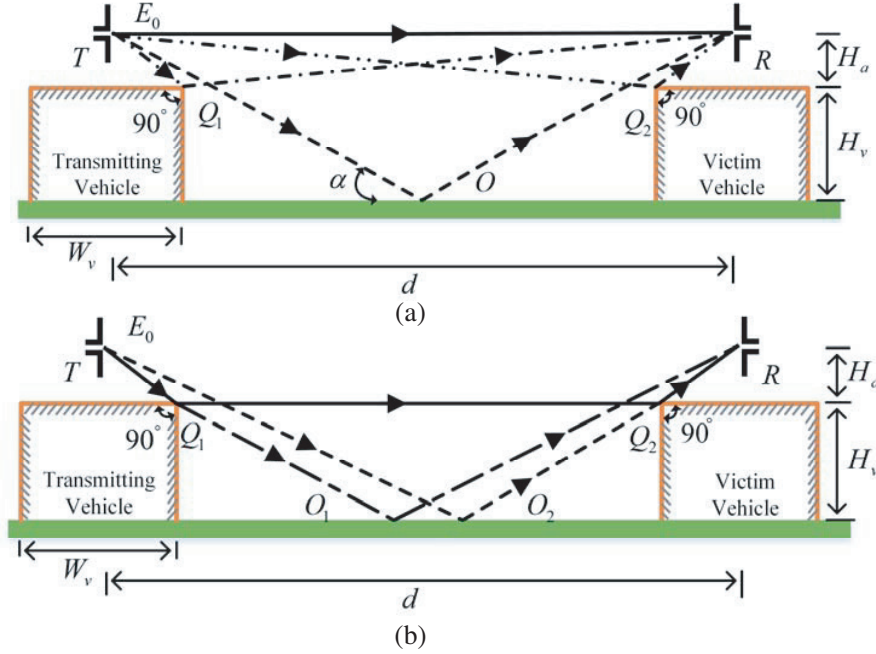


Figure 1. Geometry view of ray paths. (a) Four rays. (b) Additional three rays.

Assuming that the transmitted electric field is E_0 , the total received field at the victim vehicle using GO and UTD can be found. For four-ray situation, the total received field is

$$E_{RT1} = E_d + E_r + E_{df1} + E_{df2} \quad (1)$$

For seven-ray situation, the total received field is

$$E_{RT2} = E_d + E_r + E_{df1} + E_{df2} + E_{df-r} + E_{r-df} + E_{ddf} \quad (2)$$

The fields of direct ray E_d , ground-reflected ray E_r , roof-diffracted ray E_{df1} , roof-diffracted ray E_{df2} , roof-diffracted-ground-reflected ray E_{df-r} , ground-reflected-roof-diffracted ray E_{r-df} , and double diffraction ray E_{ddf} can be expressed as

$$E_d = E_0 \frac{e^{-jkr_d}}{r_d} \quad (3)$$

$$E_r = E_0 R_g \frac{e^{-jkr_r}}{r_r} \quad (4)$$

$$E_{df1} = E_0 \frac{e^{-jks'_1}}{s'_1} D(Q_1) \sqrt{\frac{s'_1}{s_1(s'_1 + s_1)}} e^{-jks_1} \quad (5)$$

$$E_{df2} = E_0 \frac{e^{-jks'_2}}{s'_2} D(Q_2) \sqrt{\frac{s'_2}{s_2(s'_2 + s_2)}} e^{-jks_2} \quad (6)$$

$$E_{df-r} = E_0 \frac{e^{-jks'_1}}{s'_1} D_1(Q_1) \sqrt{\frac{s'_1}{s_3(s'_1 + s_3)}} e^{-jks_3} R_{g1} \frac{e^{-jkr_1}}{r_1} \quad (7)$$

$$E_{r-df} = E_0 \frac{e^{-jkr_2}}{r_2} R_{g2} \frac{e^{-jks'_4}}{s'_4} D_1(Q_2) \sqrt{\frac{s'_4}{s_2(s'_4 + s_2)}} e^{-jks_2} \quad (8)$$

$$E_{ddf} = E_0 \frac{e^{-jks'_1}}{s'_1} D_2(Q_1) \sqrt{\frac{s'_1}{s(s'_1 + s)}} e^{-jks} D_2(Q_2) \sqrt{\frac{s}{s_2(s + s_2)}} e^{-jks_2} \quad (9)$$

where k is the wavenumber in free space, $r_d = \overline{TR}$, $r_r = \overline{TOR}$, $s'_1 = \overline{TQ_1}$, $s_1 = \overline{Q_1R}$, $s'_2 = \overline{TQ_2}$, $s_2 = \overline{Q_2R}$, $s_3 = \overline{Q_1O_1}$, $r_1 = \overline{O_1R}$, $r_2 = \overline{TO_2}$, $s'_4 = \overline{O_2Q_2}$, $D(Q_1)$, $D(Q_2)$, $D_1(Q_1)$, $D_1(Q_2)$, $D_2(Q_1)$, and $D_2(Q_2)$ are the dyadic diffraction coefficients [11], R_{g1} , R_{g2} , and R_g are the ground reflection coefficients which depend on the angle of incidence, ε_r , and σ [12]. For vertical polarization the ground reflection coefficient can be expressed as

$$R_g = \frac{(\varepsilon_r - jx) \sin \alpha - \sqrt{(\varepsilon_r - jx) - \cos^2(\alpha)}}{(\varepsilon_r - jx) \sin \alpha + \sqrt{(\varepsilon_r - jx) - \cos^2(\alpha)}} \quad (10)$$

where $x = \sigma/\omega\varepsilon_0$, ω is the angular frequency, ε_0 the dielectric constant of free space, and α the angle of incidence.

Assuming that the ideal received power at the victim antenna in free space is P_0 , in far-field condition the relationship between the transmitted power P_T and the received interference power in real environment is given by

$$\begin{cases} P_I = P_0 \left| \frac{E_{RT}}{E'_0} \right|^2 \\ P_0 = \frac{P_T G_T G_V \lambda^2}{(4\pi d)^2} \\ E'_0 = E_0 \frac{e^{-jkd}}{d} \end{cases} \quad (11)$$

where $E_{RT} = E_{RT1}$ for four-ray situation, $E_{RT} = E_{RT2}$ for seven-ray situation, E'_0 is the field strength at the victim antenna in free space, λ the wavelength in free space, G_T the transmitting antenna gain in the direction of the victim antenna, and G_V the victim antenna gain in the direction of transmitting antenna. As a result, the received interference power in decibels can be expressed as

$$P_I = P_T \text{ (dBm)} + G_T \text{ (dB)} + G_V \text{ (dB)} + 20 \log_{10} \left(\frac{\lambda}{4\pi} \left| \frac{E_{RT}}{E_0} \right| \right) \quad (12)$$

We next investigate the performance of the presented method. Full-wave simulations are carried out to confirm the validity of the proposed method. A full-wave solver of FEKO [13], using the method of moments (MoM) is employed to solve the large-scale problem discussed in this paper. Representative antennas such as omnidirectional dipole and directional microstrip patch antenna are considered. The profiles of both antennas are displayed in Figure 2(a). The dipole works at 450 MHz with 0.28 m in length. The operating frequency of the microstrip patch antenna is 1.2 GHz, which is probe fed. The radiating patch has dimensions of $80.3 \times 89 \text{ mm}^2$, and the size of the substrate is $160 \times 160 \text{ mm}^2$. The thickness and dielectric permittivity of the substrate are 2 mm and 2.2. The values of antenna gain are 2 and 7.4 dB for dipole and patch antenna, respectively. Dimensions of the vans used in simulations are shown in Figure 2(b) with $W_v = 1.85 \text{ m}$ and $H_v = 3 \text{ m}$. The vehicle body is modeled by perfect electric conducting (PEC), the windows are modeled by lossless glass with $\varepsilon_r = 4.5$, and the tires are modeled by lossless rubber with $\varepsilon_r = 2.2$ [14]. In addition, the ground environment is assumed to be infinite in FEKO simulations, and the infinite ground is modeled by means of reflection coefficient approximation. $H_a = 0.6 \text{ m}$ are chosen for the case of dipole; $H_a = 0.2 \text{ m}$ are adopted for the case of microstrip patch

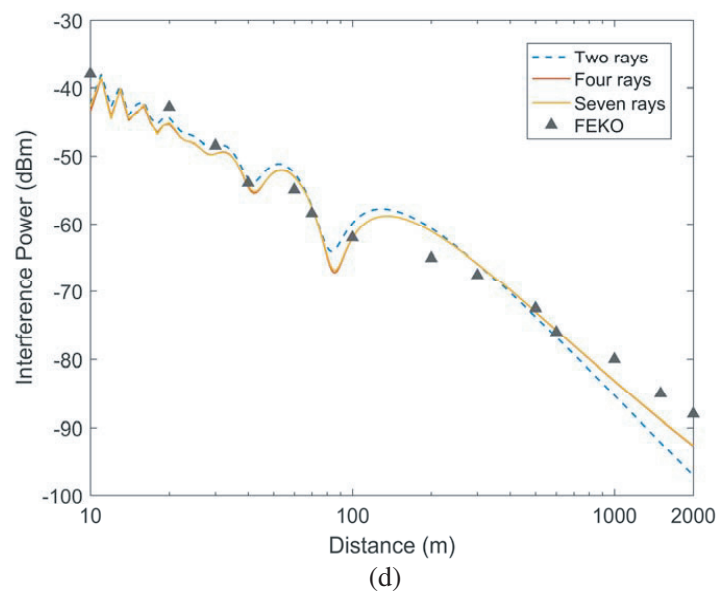
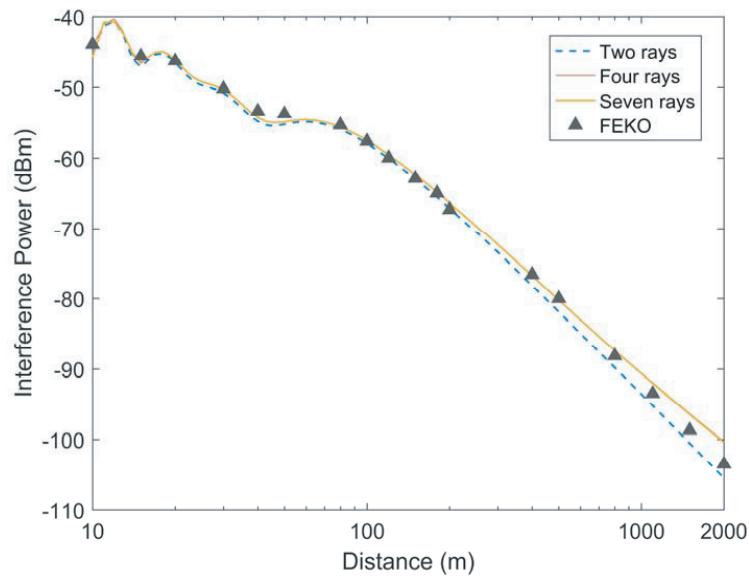
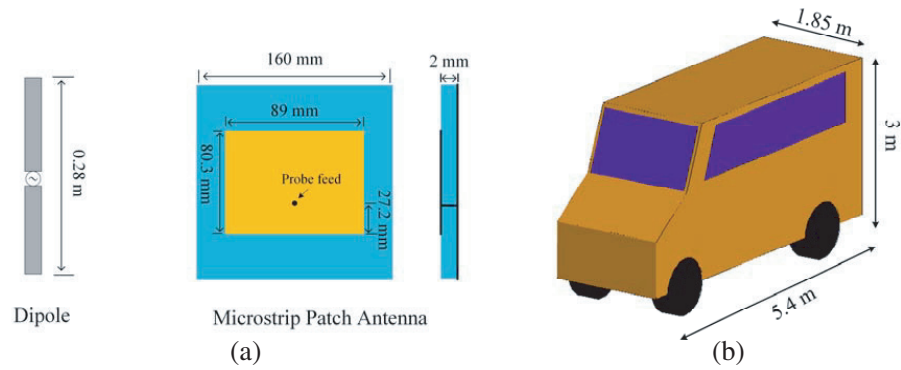


Figure 2. Profiles of antennas and vehicle in simulations and prediction comparisons with full-wave simulations. (a) Antenna profiles. (b) Vehicle profiles. (c) The case of dipole. (d) The case of patch antenna.

antenna in simulations. Note that (12) is valid for far-field. The distance d between the two vehicles should be larger than three wavelengths for wire antennas and $2D^2/\lambda$ (D is the maximum overall dimension) for patch antennas to satisfy the far-field condition. Hence, in this paper d is performed starting at 10 m. The predicted results using four-ray and seven-ray theory are shown in Figures 2(c) and (d). The predicted results using two-ray theory are also shown for comparison. The value of 0 dBm is assumed at the transmitting antenna; the average ground ($\epsilon_r = 15$ and $\sigma = 0.005$ S/m) [12] is adopted to determine the ground reflection coefficients. Compared to the results using four rays, the seven-ray model has negligible effect on the prediction accuracy. That means a larger number of rays will not change the prediction. It can also be seen that the use of two-ray model is not accurate enough for prediction especially at large distance and an improvement of about 5 dB can still be obtained. Clearly, the interference power can be predicted by means of four-ray theory. From Figures 2(c) and (d), it is observed that the FEKO simulations show good agreement with the theoretical lines for both antennas. The difference between the proposed method and full-wave simulation could be because the mesh size used in full-wave simulation is slightly coarse. In order to reduce the computation time and memory costs, the mesh size is 1/4th of wavelength as full-wave simulations require huge computational resources to solve this electrically large problem.

Measurements are conducted to further verify the proposed four-ray method. The performance of the proposed four-ray model is tested in two different environments: concrete road and wet ground. The real pictures of measurement sites are shown in Figure 3. Two vans with 5.4 m in length, 1.85 m in width, and 3 m in height are used. In measurements, a dipole, a signal generator, and a high power amplifier are used in the transmitting vehicle. The gain of the omnidirectional dipole at 450 MHz is 2.1 dB, and the transmit power is 35 dBm. In the victim vehicle, a directional log-period antenna (LPDA) with a gain of 4.3 dB at 450 MHz is used. These two antennas are chosen as they exhibit different radiation pattern. In measurements, the antennas are placed with 0.8 m above the roof and the LPDA is oriented with its maximum radiation direction toward the dipole. The interference power is measured by means of a spectrum analyzer. Due to the limitation of the measurement sites, the maximum distance measured is 200 m. The predictions using the four-ray approach are calculated based on the following two sets of constitutive parameters: $\epsilon_r = 2.35$ and $\sigma = 0.003$ S/m; $\epsilon_r = 25$ and $\sigma = 0.02$ S/m for concrete road and wet ground, respectively [10, 12]. Figures 4 and 5 show the measured and predicted interference power. We can see that the predicted results closely match the measured results. These slight discrepancies between the measurements and the theoretical results can be attributed to three factors. First, we do not know exactly the relative permittivity and conductivity of the ground in measurements. Second, the ground is not perfectly smooth and scattering is inevitable. Third, there exist electromagnetic emissions from unintentional sources outdoors as the electromagnetic environment in measurement is not pure. From the data shown in Figures 4 and 5, it can be concluded that the presented four-ray model is suitable for EMI prediction.



Figure 3. Pictures of measurement sites. (a) Concrete road. (b) Wet ground.

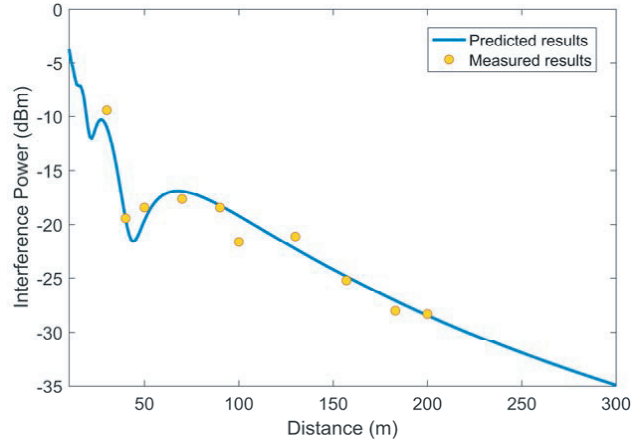


Figure 4. Measured and predicted results for concrete road environment.

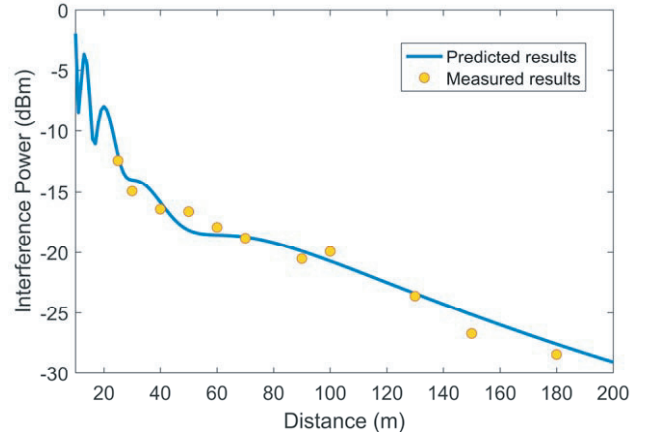


Figure 5. Measured and predicted results for wet ground environment.

3. PARAMETRIC STUDIES

After validation of the proposed four-ray method, four parametric studies are presented. First, the effects of vehicle height (H_v) and antenna height (H_a) on the interference power are studied. The second study emphasizes the effects ε_r and σ on the interference power.

3.1. Effects of Vehicle Height and Antenna Height

The effects of varying H_v and H_a on the received interference power at the victim antenna are shown in Figures 6 and 7. Figure 6 shows the interference power for a range of H_v and $H_a = 0.4$ m; Figure 7 shows the interference power for a range of H_a and $H_v = 1.5$ m. It should be pointed out that there exists a critical distance d_c . Before that, the ground-reflected ray vanishes. From Figure 1, geometry gives $d_c = W_v(H_a + H_v)/H_a$. Hence, for $d < d_c$, the total received field at the victim antenna is $E_{RT} = E_d + E_{df1} + E_{df2}$. From Figures 6 and 7, it is interesting to note that there also exists the break point [15] for the proposed four-ray situation. This is mainly because the contributions of the roof-diffracted rays E_{df1} and E_{df2} are relatively small when compared to the direct and ground-reflected

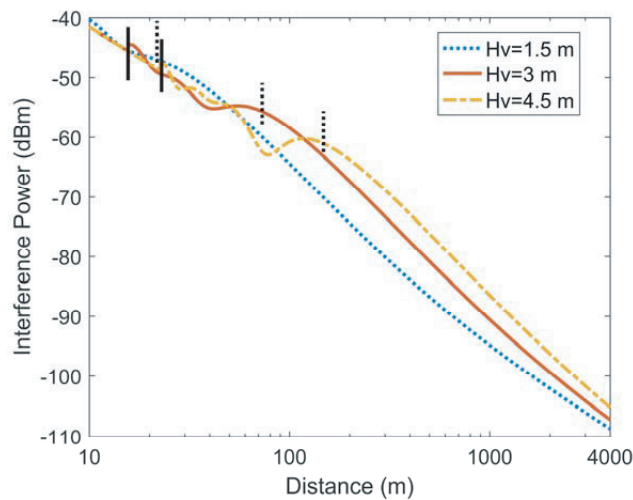


Figure 6. Interference power for different vehicle heights.

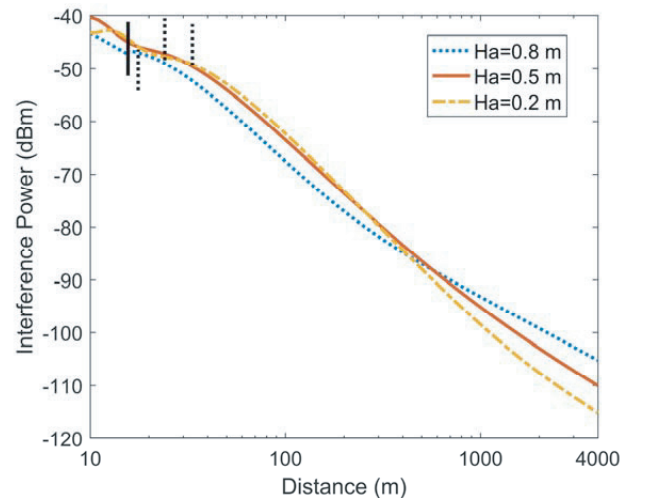


Figure 7. Interference power for different antenna heights.

rays. The characteristic of the two-ray theory is not significantly affected by the additional two rays. Thus, the break point will remain unchanged and can be written as $d_b = (16(H_v + H_a)^2 - \lambda^2)/4\lambda$ [15]. Clearly, the received interference power can be separated into three regions if $d_b > d_c$; the received interference power can be separated into two regions if $d_c > d_b$. In the following figures, the vertical solid lines and dotted lines indicate the locations of d_c and d_b , respectively.

From Figure 6, we observe that the interference power decreases steadily with distance for $d < d_c$, just as in free space. This is mainly due to the disappearance of the ground-reflected ray. For the case of $d_c < d < d_b$, the interference power exhibits fluctuation due to the destructive and constructive combination of the direct and ground-reflected rays. For the case of $d > d_b$, a rapid falloff of the interference power is observed, and higher vehicle and antenna heights lead to smaller interference power. Note that the roof-diffracted fields keep unchanged when vehicle height is varied. From Figure 7, similar results are observed when $d < d_b$. However, after d_b , the curves of interference power intersect as d increases. This is mainly due to the contributions of the roof-diffracted fields which are quite different for various H_a . As d further increases, the interference decreases rapidly again. In short, the interference power decreases with increasing H_v and H_a at large distance.

3.2. Effects of Relative Permittivity and Conductivity

As can be seen from Eqs. (1), (4) and (12), the interference power is closely related to the ground reflection coefficient which is dependent of ϵ_r and σ . Thus, it is instructive to investigate the influence of ϵ_r and σ on the received interference power. Different ground environments may have different ϵ_r and σ . For example, ϵ_r is varied from 4 to 7 and $\sigma = 0.001$ S/m for dry ground; ϵ_r is equal to 81 and $\sigma = 5$ S/m for sea water [12]. To investigate the influence of ϵ_r and σ on the interference power, a wide range of ϵ_r and σ is used. ϵ_r is varied from 2 to 82, and σ is varied from 0.001 S/m to 5 S/m.

Figure 8 shows interference power for various ϵ_r with $\sigma = 0.01$ S/m. It is observed that the interference power decreases with increasing permittivity around the break point. However, for large distance (near-grazing incidence), the relative permittivity has little effect on the interference power. Figure 9 shows interference power for various σ with $\epsilon_r = 15$. It can be seen that the interference power decreases with increasing conductivity. We also find that the interference power nearly remains unchanged for small values of conductivity varying from 0.001 to 0.1 S/m. This is mainly because small values of conductivity have very little effect on the ground reflection coefficient, which can be easily found from (10). Similarly, the effect of conductivity is not significant for large distance. This phenomenon can also be explained using (10). Note that the angle of incidence α is nearly zero for large distance. Hence, for near-grazing incidence the ground reflection coefficient is equal to -1 , and the permittivity and conductivity do not affect the received interference power.

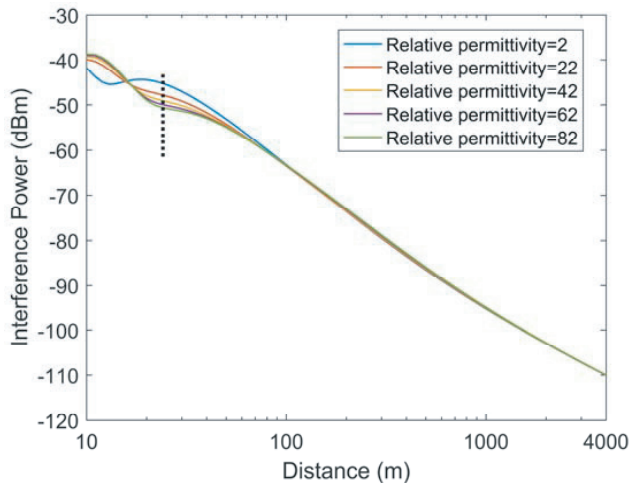


Figure 8. Interference power for various relative permittivities.

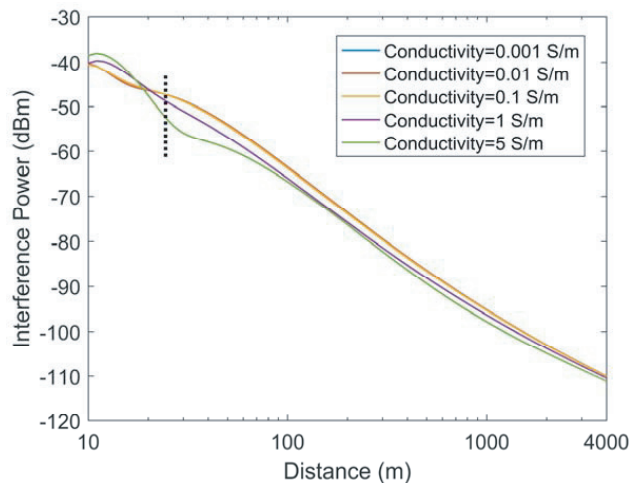


Figure 9. Interference power for various conductivities.

4. CONCLUSION

In this paper, based on theoretical analysis and measurements, we find that the presented four-ray model can predict electromagnetic interference between antennas on vehicles accurately. The relationships between the interference and the vehicle height, antenna height, relative permittivity, and conductivity are also studied. These parameters affect the interference power in different ways. The presented method can be easily used in practice for EMI prediction in various environments.

REFERENCES

1. Lopez, D. G., M. Ignatenko, and D. S. Filipovic, "Eigenmode prediction of high RF exposure frequency region inside vehicles," *IEEE Trans. Electromagn. Compat.*, Vol. 59, No. 1, 43–47, 2017.
2. Wang, H., V. Khilkevich, Y. J. Zhang, and J. Fan, "Estimating radio-frequency interference to an antenna due to near-field coupling using decomposition method based on reciprocity," *IEEE Trans. Electromagn. Compat.*, Vol. 55, No. 6, 1125–1131, 2013.
3. Gao, S. P., H. Zhao, H. W. Deng, B. F. Wang, and W. J. Zhao, "Estimating interference to airborne patch antenna with limited information," *IEEE Trans. Electromagn. Compat.*, Vol. 58, No. 2, 631–634, 2016.
4. Harris, J. M. and R. J. Levin, "Far-field techniques for predicting aircraft antenna coupling," *IEEE 1992 International Symposium on Electromagnetic Compatibility*, 112–115, 1992.
5. Frid, H., H. Holter, and B. L. G. Jonsson, "An approximate method for calculating the near-field mutual coupling between line-of-sight antennas on vehicles," *IEEE Trans. Ant. Propag.*, Vol. 63, No. 9, 4132–4138, 2015.
6. Yang, B., C. R., Birtcher, and C. A. Balanis, "The effects of passengers on mutual coupling in a simplified fuselage: Simulations and measurements," *IEEE Trans. Electromagn. Compat.*, Vol. 50, No. 3, 751–755, 2008.
7. Zhou, Q., Y. J. Xie, and Z. Chen, "Prediction of equipment-to-equipment coupling through antennas mounted on an aircraft," *Journal of Electromagnetic Waves and Applications*, Vol. 21, No. 5, 653–663, 2007.
8. Chen, Z., Y. Xie, R. Yang, J. Li, and J. Zhang, "A new approach for prediction of the mutual coupling between antennas on a complex platform," *Journal of Electromagnetic Waves and Applications*, Vol. 22, No. 8–9, 1205–1213, 2008.
9. Michael, L. B. and M. Nakagawa, "Interference characteristics in inter-vehicle communication from oncoming vehicles," *IEEE VTS 50th Vehicular Technology Conference, 1999, VTC 1999 — Fall*, 753–757, 1999.
10. Schipper, T., S. Prophet, M. Harter, L. Zwirello, and T. Zwick, "Simulative prediction of the interference potential between radars in common road scenarios," *IEEE Trans. Electromagn. Compat.*, Vol. 57, No. 3, 322–328, 2015.
11. Kouyoumjian, R. G. and P. H. Pathak, "A uniform geometrical theory of diffraction for an edge in a perfectly conducting surface," *Proc. IEEE*, Vol. 62, No. 11, 1448–1461, 1974.
12. Parson, J. D., *The Mobile Radio Propagation Channel*, 2nd edition, Wiley, NY, 2000.
13. FEKO: Version 7.0.1, [Online], Available: <https://www.feko.info/>.
14. Ulaby, F. T., E. Michielssen, and U. Ravaioli, *Fundamentals of Applied Electromagnetics*, 6nd edition, Prentice Hall, Boston, Massachusetts, 2010.
15. Xia, H., H. L. Bertoni, L. R. Maciel, A. Lindsay-Stewart, and R. Rowe, "Radio propagation characteristics for line-of-sight microcellular and personal communications," *IEEE Trans. Antennas Propag.*, Vol. 41, No. 10, 1439–1447, 1993.